Swing arm profilometer: improving the testing accuracy of large mirrors with shorter arms

Xiao Luo (罗 霄)

Key Laboratory of Optical System Advanced Manufacturing Technology, Changchun Institute of Optics, Fine Mechanical and Physics, CAS, Changchun 130033, China

Corresponding author: pb02009061@163.com

Received January 3, 2014; accepted March 15, 2014; posted online October 20, 2014

Swing arm profilometer is a useful metrology tool for large optics. For larger mirrors, the testing accuracy decreases as the arm becomes longer, while the testing accuracy requirement remains the same. We introduce a simple solution to make testing of large mirrors with shorter arms possible, which improves the testing accuracy, especially reduces the uncertainty of low-order shapes like astigmatism and trefoil. Simulation and experiment results show that testing uncertainty of low-order shape and high-frequency errors reaches 0.1 μm RMS, which faithfully meets the requirement of profile testing to guide the grinding and coarse polishing process.

OCIS codes: 220.1250, 220.4610, 220.4840.

doi: 10.3788/COL201412.S22202.

The Swing arm profilometer (SAP), invented by the Steward Observatory Mirror Lab, is one of the solutions to meet the profile testing requirement of large mirrors in fine grinding and coarse polishing phase. When compared with an ordinary commercial coordinate measuring machine (CMM), SAP performs better owing to following reasons[1–4]:

(1) The distance traveled by the probe is only as long as the amount of asphericity in the mirror, which allows the use of high-accuracy length sensors.
(2) Sources of mechanical error are removed to maximum extent (only one movement left: the rotation of the arm which holds the sensor), whereas it can be limited in sub-micros with highly accurate air rotary bearings.
(3) With an optical, non-contact sensor, SAP can measure continuously, which increases the amount of testing data significantly and decreases the effect of noise.

Till date, the largest mirror tested by SAP is a 1.4 m convex asphere at University of Arizona with a 1.5 m arm. If a 4 m mirror needs to be tested using this technology, a 3 m swing arm is required. Compared with a 1.5 m arm, a 3 m arm doubles the error from air bearing, and it is more sensitive to environment perturbations like vibration, temperature change and air turbulence. Owing to this, the testing accuracy becomes worse with longer arms; but for larger mirrors, the testing accuracy requirement remains the same. So, if SAP is used to test larger mirrors, building a longer arm is not a suitable option.

We introduce a simple way to enable the profile testing of large mirrors with relatively shorter arms. With this method, a 1 m arm is sufficient to test a 4 m mirror. Shorter arms could improve the accuracy of testing in two ways:

(1) Shorter arms result in smaller errors due to run-out of air bearing, encoder error and vibration.
(2) Shorter arms have large arc covering the surface, which could reduce the testing uncertainty of low-order errors such as astigmatism and trefoil.

Both software simulation and experiment are performed based on this idea. Results show that the accuracy of testing is within 0.1 μm RMS, which is sufficient to guide the fabrication of large optics.

The testing theory of the SAP is based on the fact that all measuring instruments have an accuracy that is proportional to their total range. By minimizing the measuring range of the testing, the testing accuracy can be improved significantly. To test an asphere, the minimum testing range is the largest aspheric departure from its best-fitting sphere[1].

In order to measure the departure from its best-fitting sphere, the sensor needs to move along the vertex sphere. This can be done by attaching an indicator to the end of a radius rod pivoted about the center of curvature between the asphere and the sphere defined by the pivot point as shown in Fig. 1(a). Unfortunately, such a scheme is difficult to implement because it becomes too long for large mirrors and the position of the rod is difficult to control.

To overcome the difficulties of the radius rod method, the geometry of a sphere generator is used for reference. In a sphere generator, a cup wheel is rotated about an axis inclined with respect to the axis of rotation of the work such that the two axes cross at the center of curvature as shown in Fig. 1(b). The angle between the axes is given by $\theta = \sin^{-1}(l/R)$, where l is the perpendicular distance from where the cup wheel rotates. Its periphery moves along an arc that appears to be generated by a radius rod pivoted from the center of curvature of the surface as shown in Fig. 1(c).

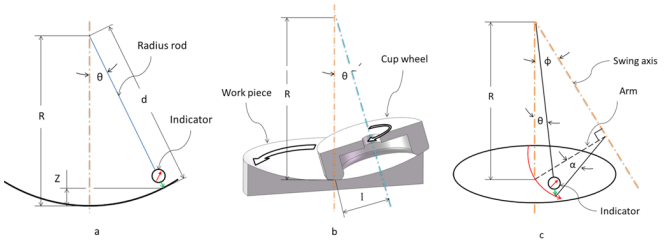

Fig. 1. (a) Indicator pivot from its center; (b) geometry of a cup wheel sphere generator; (c) geometry of a profilometer.

Anderson *et al.* were the first to report on SAP in 1990. At that time, they used mechanical touch probe that swings across the optic under test to provide a profile.

In 2009, Su reported enhancement of the swing-arm profilom with an optical interferometric probe and full two-dimensional capability, so that non-axisymmetric error can be measured. This feature is required for the production of off-axis aspherics and free-form optics[3].

Figure 2 shows the basic geometry of the swing-arm profilom. A probe is mounted at the end of an arm that swings across the optic under test such that its axis of rotation goes through the center of curvature of the optic. The arc defined by the probe tip trajectory, for a constant probe reading, lies on a spherical surface defined by this center[1,2].

As the indicator sweeps across the spherical surface, it would not show run-out with a perfectly stiff arm and perfect bearing. The angle of the required tilt is given by:

$$\sin \theta = l/R, \tag{1}$$

where l is the length of the arm and R is the radius of curvature of the sphere.

In order to measure aspheric surface, the probe that is aligned parallel to the normal to the optical surface reads only the surface departure from spherical. The swing arm geometry works for convex, concave, and plane parts. For measuring concave parts, the scan angle need to be only tilted toward the optic, rather than away from the optic as shown for the convex measurements.

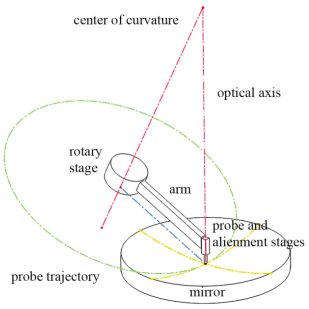

Fig. 2. The basic geometry of the swing-arm profilom. The probe is mounted on arm pivoting about the rotary stage. The rotation axis of the swing-arm is aligned to intersect the center of curvature of the surface.

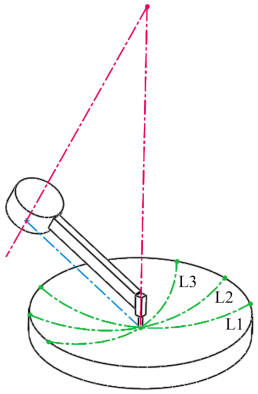

Fig. 3. Multiple scans of the mirror to create full surface maps.

This geometry can be used to scan across the diameter of the surface. Multiple scans can be combined by using data from circumferential scans by rotating the substrate under the probe as shown in Fig. 3.

A previous work has shown that the effect of misalignment on testing accuracy is negligible. The primary source of error is the rotary bearing, which carries the arm pivoting over the optical surface. Axial run-out couples directly with the measurement and the tilt run-out movement of the air bearing is magnified by the arm[2]. Air bearings with axial run-outs of the order 1 μ rad produce about 1 μm error in the measurement over a 1 m arm length. If these errors are repeated, they can be calibrated by measuring a known standard such as a spherical surface.

Random error of SAP testing caused by vibration, air turbulence or temperature change causes low-order errors like astigmatism and trefoil. A MATLAB program is written to analyze the effect of the arm length on the testing accuracy, especially on low-order errors. To simplify the simulation, the effect of misalignment, aspheric departure is ignored, only the effect of noise is considered in the simulation. The program simulates the testing of a 4 m flat, and different arm lengths are simulated in the program.

When the mirror rotates, the measuring errors are introduced in the table carrying the mirror. As a result, different arcs cannot be put together directly. Three chief errors need to be considered in this test; there are tip/tilt of the mirror and translation of the mirror along the symmetry axis of the mirror. These errors have the same effect as that of the center of the mirror curvature decenter.

As shown in Fig. 4, if the decenter direction is Y, then the test error caused by this error is a tilt. If the decenter direction is X, the form of test data error is a power, and if the decenter direction is Z, it will bring a piston in the testing data.

When the arcs cross each other as the sensor scans the mirror edge to edge, the surface heights must be the same at these scan crossings. This crossing height information is used to stitch the scans into a surface

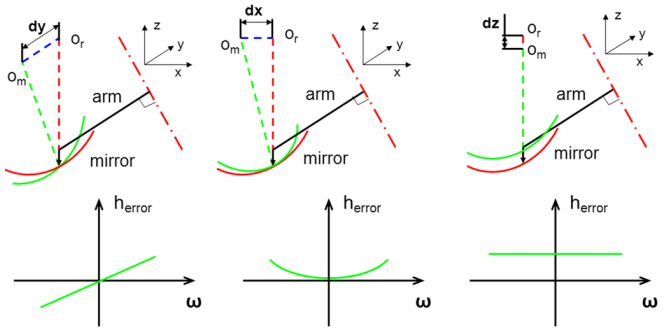

Fig. 4. Effects of the run-out of the rotating table supporting the mirror on the scan results.

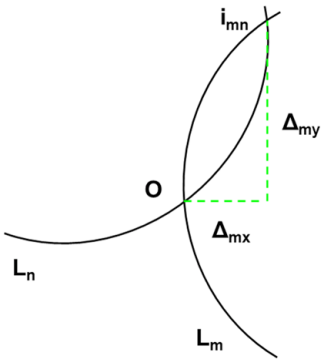

Fig. 5. The projection of lines m and n on the surface perpendicular to the axis of the rotating table under the mirror.

and the movement of the mirror between testing in different directions can be calculated.

Based on this idea, a function can be written, as shown in Fig. 5, for the point I_{mn} where line m and line n cross. The testing data plus the height change caused by motion of the mirror between nth and mth test should be equal:

$$V_{mi} + C_{mi} = V_{ni} + C_{ni}, \tag{2}$$

$$C_{mi} = dx_m \times \Delta x_{mi}/R + dy_m \times \Delta y_{mi}/R + dz_m, \tag{3}$$

$$C_{ni} = dx_n \times \Delta x_{ni}/R + dy_n \times \Delta y_{ni}/R + dz_n, \tag{4}$$

where V_{mi} and V_{ni} are the testing values of lines m and n at crossing point I_{mn}, C_{mi} and C_{ni} are the height changes caused by error motion of the mirror, dx, dy, and dz are the equivalent position changes of the center of the mirror, Δx is the distance between point I_{mn} and line OO′, Δy is the distance between point I_{mn} and point O in the direction of line OO′, and R is the radius of the mirror.

There are three variations for every line, and every two lines share a cross point, so at least six cross points are needed to solve the functions. At the same time, there are some global boundary conditions for the problem.

Suppose the height of the center point is 0, so for every scan.

$$V_{m0} + C_{m0} = 0, \tag{5}$$

where V_{m0} is the tested value for line m and C_{m0} is the error motion caused by mirror rotation.

There is no tilt of the error map of the mirror:

$$\begin{cases} \sum_{m=0}^{N-1} dx_m \times \cos(2m\pi/N) = 0, \\ \sum_{m=0}^{N-1} dy_m \times \sin(2m\pi/N) = 0. \end{cases} \tag{6}$$

There is no power of the error map:

$$\sum_{m=0}^{N-1} dy_m = 0. \tag{7}$$

With these equations, we can solve variables, remove the effect of the motion of the mirror on dataset tested, and then we can have a best estimate of the error map of the mirror.

A Monte-Carlo simulation of the SAP with Matlab program was performed assuming 0.1 μm RMS uncertainty at each measurement point, with 48 scans and 100 points per scan. The mirror under test is a Φ 4 m flat. Figures 6 and 7 show the distribution of data points with different arm length. Two cases are discussed here:

Case A: the uncertainty of each data is fixed to be 0.1 μm RMS. This happens when the error of air bearing is a pure piston movement.

Case B: the uncertainty of each data is 0.1 μm multiplied by the length of the arm (in m). This simulates

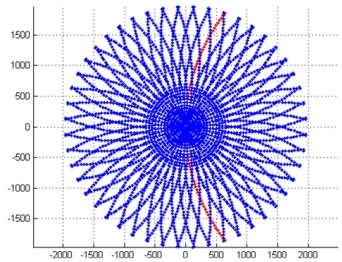

Fig. 6. SAP profiling pattern of a 4 m mirror with arm length of 3 m.

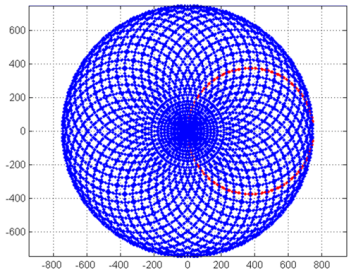

Fig. 7. SAP profiling pattern for a 4 m mirror with arm length of 1 m.

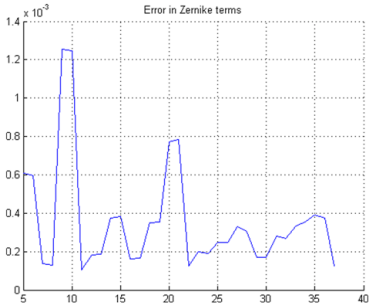

Fig. 8. RMS uncertainty of low-order Zernike aberrations with arm length of 3 m (unit in mm).

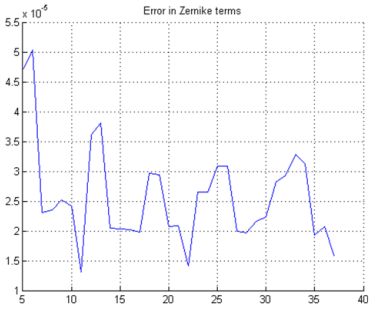

Fig. 9. RMS uncertainty of low-order Zernike aberrations with arm length of 1 m (unit in mm).

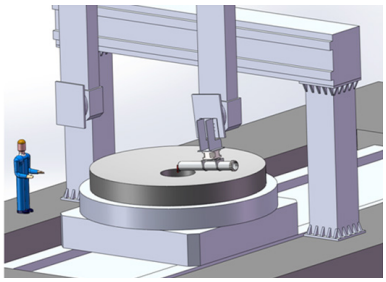

Fig. 10. A 3-D model of the 4 m CNC grinding/polishing machine with an *in situ* SAP. There are two *Z* axes, one for testing and other for fabrication.

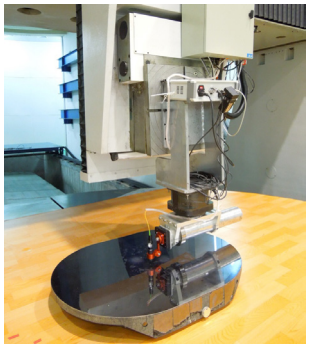

Fig. 11. SAP *in situ* measuring the 1000×800 mm sphere mirror.

the condition when the error movement of the air bearing is a pure tilt.

What really happens is somewhere between case A and case B. As the arm gets longer, it will be more close to case B and more close to case A when the arm gets shorter. Four kinds of arm lengths from 1 to 3 m are calculated and the results are listed in Table 1.

The uncertainty of low-order Zernike aberrations is plotted as functions of the Zernike modes as shown in Figs. 8 and 9. For the case of arm length of 1000 mm, the surface can be determined as 42 nm RMS.

The uncertainty of testing can be reduced about 10 times if we use a 1 m arm instead of a 3 m arm. This can be implemented by hanging the SAP above the mirror rather than placing it beside the testing mirror.

This result is easy to understand. For a 3 m arm, there are only 9 cross points for each arc, but for a 1 m arm, it has 2 cross points almost with every other arcs, 93 cross points in total. More cross points indicate more information, which could reduce the uncertainty of testing.

A round square sphere of dimension of 1080×820 is tested with this particular new SAP design. The arm is fixed on the spindle of a 4 m CNC grinding/polishing machine, as shown in Figs. 10 and 11. The machine has a 4 m rotating table, which is used to place and rotate the mirror. *B*-axis on the spindle is used to generate the tilt angle θ of the arm, and *XYZ* slide axes are used to adjust the arm's position.

During the test, the sphere was scanned in 48 equally spaced arcs. Each arc was scanned eight times to average out the noise. The arm length is 299.78 mm, slightly longer than the one-fourth of the length of the long axis of the mirror.

Table 1. PV/RMS Uncertainty of Low-order Zernike Aberrations with Different Arm Lengths (μm)

Condition	**Arm Length (μm)**							
	1000		**1500**		**2000**		**3000**	
	PV	RMS	PV	RMS	PV	RMS	PV	RMS
Case A	0.42	0.06	1.0	0.11	1.8	0.20	2.3	0.27
Case B	0.42	0.06	1.5	0.17	3.6	0.40	7.0	0.82

Figure 12 shows one of the original testing data averaged with eight sets of raw data and Fig. 13 shows the residual data and uncertainty of data with the error moments of swing arm removed; the average noise of the testing is 25 nm. It is measured by subtracting the average of many scans from a single scan. Figure 14 shows the departure of a single scan from the mean of dataset and Fig. 15 shows the profiling pattern for the 1080×800 shpere under experiment.

The testing data are processed with the method described in above; the shape of the mirror is reconstructed and the results are shown in Fig. 16.

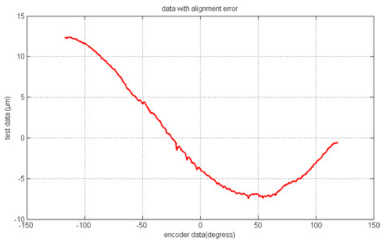

Fig. 12. Data of a single scan with alignment error.

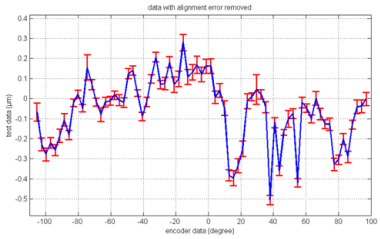

Fig. 13. Data of a single scan with alignment error removed.

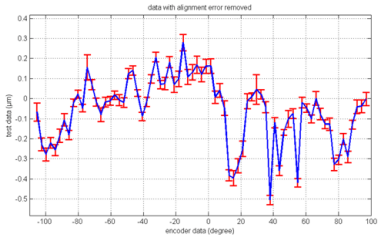

Fig. 14. Departure of a single scan from mean of dataset.

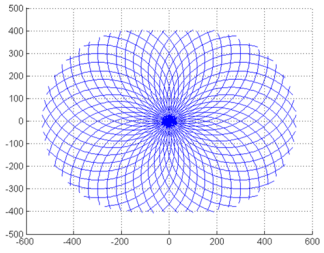

Fig. 15. Profiling pattern of 1080×800 mm sphere under test.

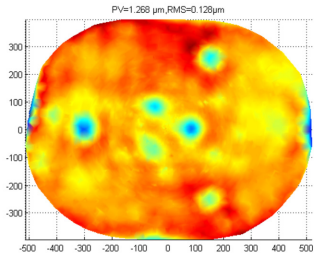

Fig. 16. SAP test result.

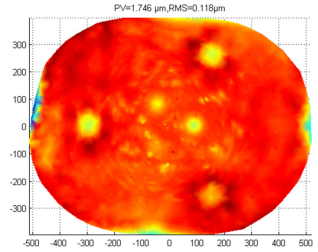

Fig. 17. Interferometric testing result.

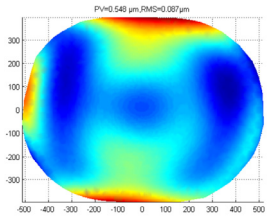

Fig. 18. Difference between SAP and interferometer test result with 37 low-order Zernike shapes.

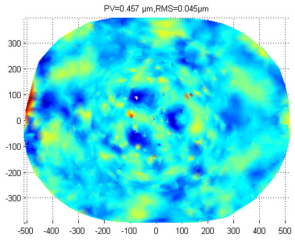

Fig. 19. Difference between SAP and interferometer test result with 37 low-order Zernike aberrations removed.

To verify the testing accuracy, the sphere is tested with an interferometer. Test results are shown in Fig. 17.

Figure 18 represents 37 low-order Zernike shapes and Fig. 19 shows the high-order error. The results show that the RMS uncertainty of low-order shapes is within 0.1 μm and for high-order error, it is within 0.05 μm without any calibration of the air bearing. The results validate that SAP with short arms is stable and the uncertainty of low-order errors is well controlled.

In conclusion, we propose a feasible method for profile testing of large optics. This new configuration makes testing of large mirrors possible with relatively shorter arms, which make it more practical and more accurate, especially on low-order shapes. The accuracy of testing of large optics reaches sub-micro, which is sufficient for guiding of grinding and coarse polishing of large optics.

References

1. D. S. Anderson, R. E. Parks, and T. Shao, in *Proceedings of OF&T Workshop Technical Digest* (Academic, Monterrey, CA, 1990), Vol. 11, pp. 119–122.
2. D. S. Anderson and J. H. Burge, Proc. SPIE **2356,** 269 (1995).
3. P. Su, C. J. Oh, R. E. Parks, and J. H. Burge, Proc. SPIE **7426,** 74260J (2009).
4. H. Jing, C. King, and D. Walker, Opt. Express **18,** 2036 (2010).